Reactive Transport Modelling of CO2 Sequestration in Saline Aquifers

Vincent Lagneau, A. Pipart, H. Catalette

Oil & Gas Science and Technology – Rev. IFP, Vol. 60 (2005), No. 2, pp. 231–247

IFP International Workshop
Rencontres scientifiques de l'IFP

Gas-Water-Rock Interactions ... / Interactions gaz-eau-roche ...

Reactive Transport Modelling of CO_2 Sequestration in Deep Saline Aquifers

V. Lagneau[1], A. Pipart[1] and H. Catalette[2]

1 Centre d'informatique géologique, École des mines de Paris, 77305 Fontainebleau Cedex - France
2 Électricité de France / Recherche et Développement, Site des Renardières,
Route de Sens, Écuelles, 77818 Morêt-sur-Loing Cedex – France
e-mail: vincent.lagneau@ensmp.fr – hubert.catalette@edf.fr

Résumé — Modélisation couplée chimie-transport du comportement à long terme de la séquestration géologique de CO_2 dans des aquifères salins profonds — La séquestration géologique de CO_2 dans des aquifères salins profonds peut présenter de nombreux atouts dans la lutte contre les émissions de gaz à effet de serre. Afin d'assurer un bon confinement du gaz injecté, une bonne compréhension de l'évolution de tels systèmes sous l'influence d'une injection massive de CO_2 est déterminante. À ce titre, les modélisations couplées géochimie-transport peuvent apporter des renseignements utiles, en simulant les réactions chimiques susceptibles de se produire dans le milieu, couplées au transport des réactifs, et ce, à long terme et à grande échelle.

Cette étude avait pour but d'explorer les apports possibles de la modélisation couplée géochimie-transport dans le cadre de la séquestration du CO_2. Deux aquifères salins profonds ont été choisis afin de tester les performances et les limitations des codes : l'aquifère carbonaté du Dogger (Bassin parisien) et l'aquifère gréseux du Bunter (mer du Nord). Ces deux aquifères aux comportements différents ont été choisis afin d'illustrer les principaux phénomènes attendus : dissolution du CO_2 dans l'aquifère carbonaté, précipitation de carbonates dans l'aquifère gréseux.

Les simulations effectuées montrent les performances des codes couplés, en particulier la possibilité de représenter finement le terme source (ou puits) de la dissolution de la bulle de CO_2 (ou de la précipitation de minéraux carbonatés) couplé au transport du CO_2 dissous. Le calcul des flux de CO_2 en divers points du système donne en outre des informations sur le potentiel de fixation du CO_2. Cependant, des limitations ont été identifiées : manque de données sur les structures modélisées et sur la réactivité du CO_2 dans les conditions envisagées. Enfin, des développements dans les codes sont également souhaitables afin de représenter plus finement le transport, la dissolution et la réactivité du CO_2 supercritique : couplage chimie-transport en milieu biphasique, couplage avec les échanges de matière entre phase.

Abstract* — *Reactive Transport Modelling and Long Term Behaviour of CO_2 Sequestration in Saline Aquifers — *Geological sequestration of CO_2 in deep saline aquifers may offer numerous opportunities for the mitigation of greenhouse gas emissions. In order to ensure good containment, a correct understanding of the evolution of such systems after a massive injection of CO_2 is compulsory. For this purpose, coupled reactive transport modelling can provide useful information, by simulating chemical reactions likely to occur in the system coupled to reactive transport, at large time and space scales.*

This study aimed at investigating the possible benefits of reactive transport modelling in the context of CO_2 sequestration. Two deep saline aquifers have been chosen to test the performance and limitations of the codes: the carbonated aquifer of the Dogger (Paris Basin) and the sandstone aquifer of the Bunter (North Sea). The aquifers, with contrasting behaviours, have been chosen to illustrate the main expected phenomena: CO_2 dissolution in the carbonated aquifer, carbonate mineral precipitation in the sandstone aquifer.

The simulations highlight the performance of the reactive transport codes, particularly the possibility to represent in detail a source (or sink) term with the dissolution of the CO_2 bubble (or the precipitation of carbonated minerals), coupled to the transport of the dissolved CO_2. Furthermore, flux assessment at various points of the system illustrates the storage capacity of the systems. However, several shortages have been identified: a lack of data on the aquifers and on the reactivity of CO_2 under sequestration conditions. Finally, developments are advisable to better estimate the transport, dissolution and reactivity of the supercritical CO_2: This involves a two-phase coupled reactive transport code, and a coupling with the exchange between phases.

INTRODUCTION

One of the major problems facing mankind is the global warming due the anthropogenic emissions of greenhouse gases. Several technological processes are already available to capture CO_2 from flue gases. The CO_2 captured must be sequestered to ensure it will not reach the atmosphere for several hundreds or thousands of years. Several sequestration scenarios are currently considered: geological sequestration, terrestrial sequestration in plants and soils, or possibly injection in deep oceans.

For geological sequestration, several scenarios are investigated (Reichle *et al.*, 1999). Among them, disposal in deep saline aquifers offers several key assets: very large volumes available combined to a wide distribution of such systems, and the possibiblity of enhanced storage potential through carbonate mineralization. Another positive point is their low economic potential; *e.g.* their strong salinity which prevents future intrusions motivated by fresh-water exploitation. Conversely, a resulting drawback is that these systems are usually poorly characterized.

Two main processes are responsible for CO_2 trapping in deep saline aquifers: hydrodynamics (of the gas- and water-phase) and mineralization (Bachu *et al.*, 1994). Hydrodynamic trapping relies on slow regional flows (to ensure longer residence times) and a low permeability overlying aquitard (to prevent upwards migration of the CO_2). A relatively high porosity is desirable (as long as it does not imply rapid flows) to provide large volumes available. Depths greater than 800 m are preferable to ensure supercritical CO_2 conditions (Bachu, 2002).

Mineral trapping offers higher sequestration potential still: the CO_2 density is generally higher in minerals than in solution (Bachu *et al.*, 1994), and once mineralized, residence times for the CO_2 are of the order of geological times. Experiments have been carried out to investigate the mineral trapping capacity of such systems (Gunter *et al.*, 1993, 1997; Kaszuba *et al.*, 2003). Conversely, the CO_2 phase or dissolved CO_2 might react with the overlying aquifer, thus deteriorating the caprock sealing properties (Rochelle *et al.*, 1999). Very few experiments are available so far, either for code feeding (thermodynamical and kinetical constants) or for code testing (benchmarking on field observations).

Experimental data are needed, but are limited in time, space and conditions. Coupled reactive transport codes thus provide a useful tool to extend the experimental results, and to predict the behaviour of the injected CO_2 in the aquifer. Reactive transport codes are widely used in a variety of domains, including nuclear waste repository safety assessment, groundwater quality, soil pollution or environmental impact of industrial complexes (*e.g.* van der Lee and De Windt, 2001).

In the field of CO_2 sequestration, some reactive transport computations can be found in the literature. A suit of problems related to CO_2 sequestration has been devised for numerical codes intercomparison (Pruess *et al.*, 2002, 2004). Several phenomena and their coupling were considered (PVT data, gas advection and diffusion, rock deformation, ...), and one of the problems addressed the geochemical evolution of a glauconitic sandstone aquifer due to CO_2 injection, though without coupling with transport. Gaus *et al.* (2003) performed PHREEQC 1D diffusive reactive transport simulations of dissolved CO_2 in the cap-rock of the Utsira aquifer (Sleipner project). Johnson *et al.* (2001) simulated the behaviour of a CO_2 injection in the Sleipner sequestration environment, with coupled geochemistry, transport and two-phase flow, using a sofware package based on NUFT (reactive transport), SUPCRT92 and GEMBOCHS (thermodynamic/kinetic databases) and Xtool (graphical post-processor). Their aim was to assess the relative trapping capacity of the several compartments (solution, mineral or structural) following several scenarios (depending on the homogeneity of the aquifer and the fracturation of the intra-aquifer shales). They acknowledge the need for further developments (particularly dissolution of the formation

water into the immiscible CO_2 phase, and improved equations of state for saline fluids), and the necessity to benchmark the codes. Finally, both studies outline the weight of kinetical reactions and the difficulty to correctly handle such reactions due to lack of data (kinetics under the specific P-T conditions, specific surface areas).

Several specific problems are faced in the field of deep aquifer CO_2 sequestration (high salinity, behaviour of the CO_2 "bubble"). We therefore carried out preliminary simulations, with the code Hytec (van der Lee, 1997; van der Lee *et al.*, 2002, 2003), in order to investigate the added-value and the limitations of reactive transport simulations for the understanding of deep aquifer disposal of CO_2. For this purpose, two aquifers have been selected, according to physical, mineralogical, and location criteria: a carbonated aquifer, located in the Dogger of the Paris Basin, and a sandstone aquifer, in the Bunter formation (North Sea). A massive injection of CO_2 has been simulated in each aquifer: the injected volume represents the amount of CO_2 released by a powerplant over its entire production life. The duration of the simulations has been fixed at 10 000 a. Apart from the evolution of the local mineralogy due to the reactive CO_2, an estimation of the dissolved carbonates fluxes has been made, through several key surfaces (CO_2 bubble surface, limit of the simulated aquifer), to evaluate the trapping potential of each aquifer.

1 REACTIVE TRANSPORT MODEL

Reactive transport models combine (bio-)geochemical reactions with hydrological processes such as advective groundwater flow, diffusion or dispersion. Among the several numerical methods available for the integration of the problem, the implicit approach (*e.g.* Steefel and Lasaga, 1994, van Cappellen and Wang, 1996) integrates the reaction equations into the transport equation and then solves the fully coupled partial differential problem (Lichtner, 1996). The approach allows for large timesteps to be used for otherwise stiff problems (Steefel and MacQuarrie, 1996). However, it involves complex mathematics and cannot readily use independently available modules.

An alternative is the operator splitting method, combined with sequential iterative approach. It has several advantages: for example the possibility to couple fully featured stand-alone codes (thus facilitating development and maintainance), or the clear opportunities for parallel computations (Hundsdorfer and Verwer, 1995). The iterative improvement of the sequential approach is generally of critical importance (Carrayrou *et al.*, 2002).

Hytec is a reactive transport code initially developed for transport of chemical solutions and colloidal matter in column systems (van der Lee, 1997). Its scope has been successively widened to include 2D flow and transport resolution coupled to most of the common features expected in a geochemical code (complexation, dissolution/precipitation, redox reactions, several models for sorption and surface complexation, ionic strength activity correction, *etc.*). The model forms part of a broader simulation platform and is currently used in France for nuclear waste safety analyses, soil pollution studies, interpretation of column experiments, migration of colloidal organics in clay formations and environmental studies in general (van der Lee *et al.*, 2002).

Hytec is based on an operator splitting algorithm, with a sequential iterative scheme. The geochemical tasks of Hytec are undertaken by Chess, a versatile geochemical module, highly optimized for the purpose of coupling with transport models (van der Lee, 1998). In this study, the flow-transport part has been solved by R2D2 (Lagneau, 2003), a 2D finite volume code, based on a centroidal voronoi mesh.

To date, Hytec cannot account for multiphase reactive flow. The following simulations have thus been carried out considering the dissolved CO_2 fraction only. However, with careful selection of the initial and boundary conditions, some of the expected behaviour of the supercritical phase have been approached. For instance, a hydro-geochemical zone has been set up, to represent the CO_2 bubble; this area feeds the solution with dissolved CO_2, at a concentration imposed by the equilibrium between saline water and a supercritical CO_2 phase. In the "fast" carbonated aquifer, this zone has been allowed to move (though without dispersion) through the simulated area.

2 PHYSICO-CHEMICAL PROPERTIES OF CO_2

2.1 Physical Properties of the Supercritical CO_2

The critical point for a pure substance is defined as the endpoint of the gas/liquid separation line in a pressure/temperature diagram. In a pressure/temperature/density diagram, this point corresponds to the end of the discontinuity between the liquid and the gas phase surface. Beyond this point, no distinction between gas and liquid can be made.

For carbon dioxide, this point is characterized by the critical pressure $P_c = 73.86$ bar, temperature $T_c = 31.1\,^{\circ}\mathrm{C}$ and density $d_c = 0.468$ (Leitner, 2000). Supercritical CO_2 thus combines gas- (*e.g.* low viscosity, typically around 10^{-4} to 10^{-3} Pa·s for supercritical gases), and liquid- (*e.g.* high density) properties. However, the supercritical fluid is liable to very large changes of density, especially close to the critical point. This behaviour must be carefully addressed, as far as immiscible two-phase (supercritical CO_2 and water) flow is considered.

In addition to its physical properties, the carbon dioxide may react with the surrounding medium: the supercrititical CO_2 is soluble in water; the dissolved CO_2 thus enters the carbonate system and may react with the host rock. In addition, the chemistry of the supercritical CO_2 phase may also be important in this context.

2.2 Chemistry of the Dissolved CO_2

The supercritical CO_2 can dissolve in the pore water. The solubility depends on several factors, among which are pressure, temperature and salinity. This has been investigated by Duan and Sun (2002) and references herein (*Figs 1 and 2*).

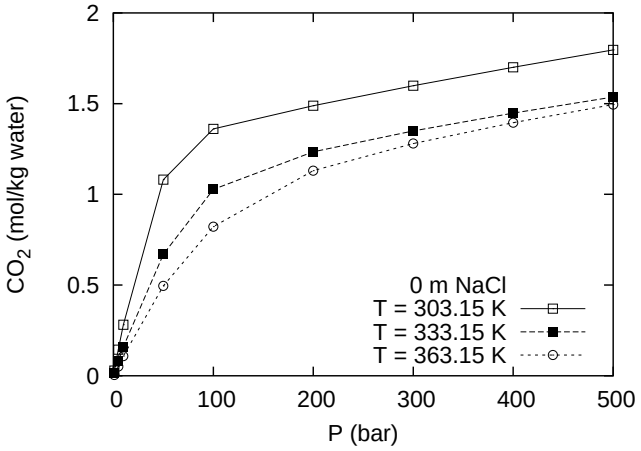

Figure 1

Solubility of CO_2 in pure water (0 molal NaCl): influence of the pressure and temperature. The CO_2 solubility increases with pressure and decreases with temperature. Data from Duan and Sun (2002).

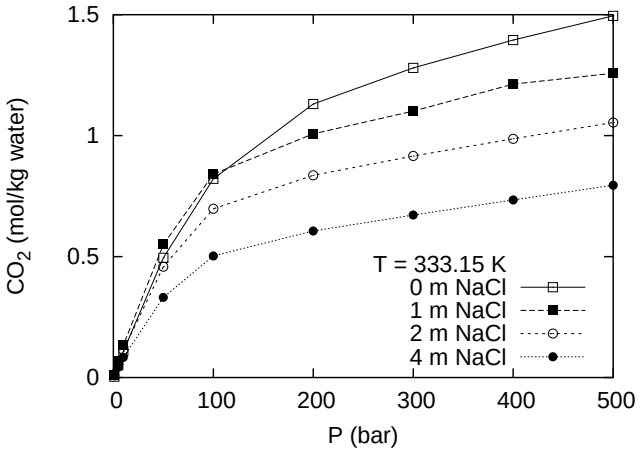

Figure 2

Solubility of CO_2 at 60 °C: influence of the pressure and salinity. At constant pressure, the solubility of CO_2 decreases with the salinity: the phenomenon is refered to as the salting-out effect. Data from Duan and Sun (2002).

The solubility of CO_2 increases with pressure, but decreases with temperature (in the examined temperature range) and the salinity. The salinity effect is known as the salting-out effect.

The dissolved CO_2 then enters the carbonate system:

$$CO_2(sc) \rightleftharpoons CO_2(aq) \quad (1)$$

$$CO_2(aq) + H_2O \rightleftharpoons H_2CO_3(aq) \quad (2)$$

$$H_2CO_3(aq) \rightleftharpoons H^+ + HCO_3^- \quad (3)$$

$$HCO_3^- \rightleftharpoons H^+ + CO_3^{2-} \quad (4)$$

The speciation of dissolved CO_2 is highly dependent on the pH (*Fig. 3*).

$CO_2(aq)$ is dominant for the lower pH, then HCO_3^- and CO_3^{2-} (resp.) become dominant for intermediate and high pH (resp.). In presence of a large amount of supercritical CO_2, the system may be considered open, as CO_2 can dissolve to

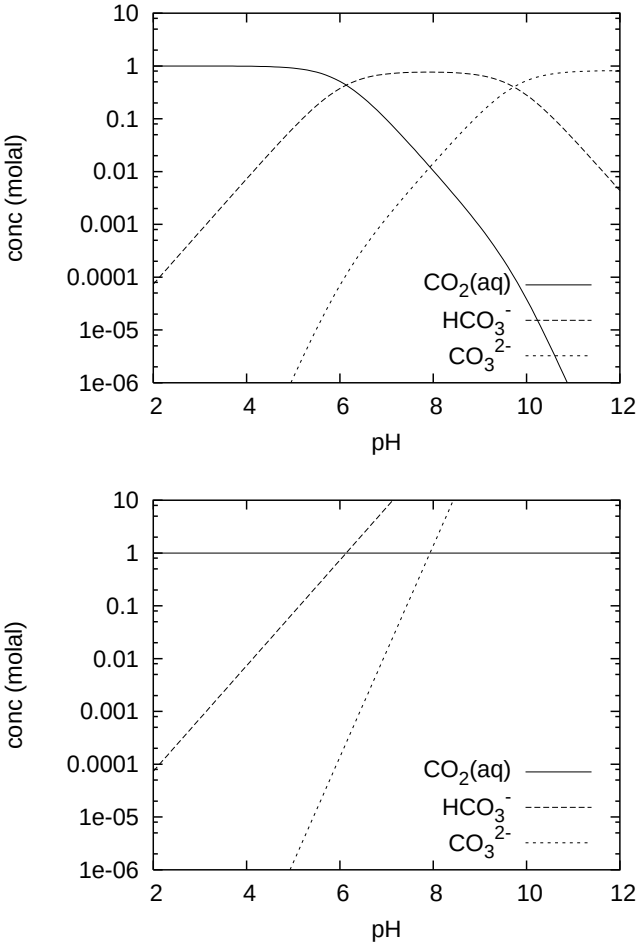

Figure 3

Speciation of the dissolved CO_2 as a function of pH, in a 1 m NaCl solution at 60 °C. For the closed system (top), the speciation evolves from dominant $CO_2(aq)$ at low pH to HCO_3^- and finally CO_3^{2-} at intermediate and high pH. For the open system (bottom), the concentration of the *species* $CO_2(aq)$ stays constant, the switch in dominant species at higher pH leads to very high concentrations in the subsequent species HCO_3^- and CO_3^{2-}.

constrain the concentration of the *species* CO_2(aq). Therefore, at intermediate or high values of pH (due to the host rock minerals buffering), the modification of the dominant carbonate species (towards HCO_3^- or eventually CO_3^{2-}) can lead to a total dissolved CO_2 concentration much larger than the concentration of the *species* CO_2(aq): higher pH leads to an apparent increase of the solubility of CO_2.

Finally, the dissolved carbonates can form soluble complexes, depending on the concentration of the co-ions: *e.g.* $CaHCO_3^+$. The complexes can shield the dissolved CO_2 and contribute to increase its total solubility.

2.3 Reactivity of the Dissolved CO_2 with the Host Rock

Once dissolved, the CO_2 can react with the surrounding minerals. A review of the minerals likely to react with CO_2 shows that they can be divided into two main classes, with opposite behaviours.

The first class of minerals offers the possibility of mineral trapping, for example in the reaction:

$$\text{anorthite} + CO_2 + 2\,H_2O \rightleftharpoons \text{kaolinite} + \text{calcite} \quad (5)$$

Minerals in this class contain calcium, magnesium, iron or other divalent ions, which can lead to the formation of carbonates. A general reaction for this class of minerals can be written as:

$$\text{silicates} + m\,CO_2 + n\,H_2O \rightleftharpoons \text{carbonates} + \text{feldspar} + \text{kaolinite} + \text{quartz} \quad (6)$$

Feldspar can further react with CO_2 to form dawsonite and quartz:

$$\text{K-feldspar} + CO_2(\text{aq}) + Na^+ \rightleftharpoons \text{dawsonite} + 3\,\text{Quartz} + K^+ \quad (7)$$

The precipitation of K-feldspar (at equilibrium) is arguable as the reaction is known to be very slow, as outlined for instance by Johnson *et al.* (2001). However, an infinitely slow K-feldspar precipitation would eventually lead to the same ultimate end-members, dawsonite and quartz (or another silicate), without the transient precipitation of K-feldspar. The reality probably stands between these two situations.

The second class gathers the carbonated minerals. These minerals cannot lead to mineral trapping, as they already contain carbonate ions. Moreover, these minerals are more soluble in acidic waters: the acidic water due to CO_2 dissolution dissolves these minerals, generating a secondary source term of carbonates. However, the carbonated minerals can efficiently buffer the pore water pH at intermediate levels, and hence increase the concentration of the total dissolved CO_2. A general reaction can be written as:

$$\text{carbonates} + CO_2 + H_2O \rightleftharpoons \text{cations} + 2\,HCO_3^- \quad (8)$$

2.4 Reactivity of the Supercritical CO_2?

The chemical behaviour of CO_2 has been widely investigated for its organic solvent properties. Supercritical CO_2 is commonly used in industry, mainly as a phase separator in supercritical fluid extraction, and more recently as an environmentally benign (*i.e.* nontoxic, greenhouse effect set aside) reaction medium (Leitner, 2000). Indeed, CO_2 is nontoxic, nonflammable, and its use is not regulated under the *Volatile Organic Compound* regulations. Besides, the reaction products can be easily recovered, without leaving any trace of the solvent, by a simple decrease in pressure.

Whilst the behaviour of supercritical CO_2 is becoming well understood in the organic chemistry, its behaviour remains largely unknown in the context of deep underground sequestration. Supercitical CO_2 is a nonpolar solvent and therefore cannot build strong solvent-solute interactions, especially with ions, as is the case for example with aqueous complexes. However, this limitation disappears with the addition of small quantities of a cosolvent (Li *et al.*, 2003).

Experiments involving supercritical CO_2 and geological materials are very scarce. Fein and Walter (1987) studied the solubility of calcite in a supercritical H_2O/CO_2 fluid, at high pressure (1 to 2 kbar), but at limited CO_2 concentrations. The experiment nevertheless shows an increase of calcite solubility with increasing CO_2 concentration, mainly due to the acidification of the fluid. But, at higher CO_2 content, as the activity of water decreases, the solubility decreases with increasing CO_2 content. This effect has been described by Joyce and Holloway (1993) who determined the activity of water in $H_2O/CO_2/NaCl$ fluids.

A very interesting experiment by Kaszuba *et al.* (2003) investigated the degradation due to supercritical CO_2 injection of a synthetic geological material at equilibrium with a saline solution. Their observations reveal an alteration of the initial minerals (dissolution of quartz, oligoclase and biotite, precipitation of magnesite, amalcine mica and several clay minerals). Additional effects have been detected, including a dehydration of the medium close to the supercritical CO_2 front. Hence, the remaining solution is enriched in sodium chloride, which could result in local very high salinity solutions or gravity-driven flow.

Thus, the effect of supercritical CO_2 injection is not limited to the dissolution of CO_2 in water and the subsequent carbonate chemistry. However, these effects are still largely unknown, and have not so far been quantified.

2.5 Implications for the Choice of Aquifers

The choice of the aquifers examined in this work has been determined by the properties of dissolved and supercritical CO_2. Several pre-requisites were established:

– supercritical CO_2 conditions to ensure very high density for the injected CO_2: temperature $> 31\,^\circ$C, pressure > 74 bar, *i.e.* an aquifer over about 800 m deep;

– large available volume, corresponding to the very large amounts of CO_2 injected;
– two types of aquifers following the expected diverging behaviour of the CO_2: on the one hand, a sandstone aquifer for its mineral trapping potential through its silicate content, on the other hand a carbonated aquifer for the expected enhanced solubility of CO_2.

In addition, the aquifer had to be within or close to the border of the French territory, and with no identified economic value. Two aquifers complied with all the criteria: the Dogger in the Paris Basin, the Bunter in the North Sea.

3 CARBONATED AQUIFER MODEL

3.1 Description of the Aquifer

The Dogger aquifer in the Paris Basin is a deep saline carbonated aquifer. It is composed of alterning Jurassic (Bajocian and Bathonian) limestones with overlying upper Aalenian to Callovian marls. The Dogger extends over the whole Paris Basin; it outcrops on the rim of the Paris Basin, from Charleville-Mézières to Neufchâteau in the East, to Poitiers in the South and Caen in the West. It dips under the Basin and extends up to the Channel. The pore water is too saline to be of any economical value: around 35 g/L equivalent NaCl.

Its properties and mineral composition are summarized in Table 1.

TABLE 1

Physical, hydrological and chemical properties of Dogger aquifer. The mineral composition is given in weight percent.

Physical properties	
Average depth	1 900 m
Average thickness	200 m
Surface area	3 500 km^2
Density	2.54 kg/m^3
Temperature	60 °C
Pressure	180 bar
Hydrological properties	
Porosity	∼ 13%
Permeability	2×10^{-5} m/s
Mean Darcy flow velocity	5 m/a
Chemistry	
Salinity	35 g/L NaCl
pH	6.3
Mineral composition	
Calcite	80%
Dolomite	7%
Illite	10%
Pyrite	3%

3.2 Model for the Dogger

The high salinity of the aquifer has several impacts on the behaviour of the system. It lowers the solubility of the CO_2 as pointed above. Also, the high Cl^- content can shield several cations, through complex formation (*e.g.* $CaCl^+$), thus increasing the effective solubility of minerals. Finally, due to the high salinity of the aquifer pore water, a model of correction of activity for ionic strength has to be used. Chess offers a variety of models (Davies, truncated Davies, Debye-Hückel, B-dot, and SIT). For this specific problem, we had to use a correction model adapted to high salinity. SIT (Specific Interaction Theory, Brønsted-Guggenheim-Scatchard, based on Brønsted, 1922) is suitable for very high ionic strength solutions; however, the model was not available in the coupled geochemistry-transport version at the time of the study. We therefore chose the B-dot model (Helgeson, 1969), which is accurate up to salinities of 1 to 1.5 molal.

3.2.1 First Model

A first simulation has been realized, on a 1D geometry, to give a thorough understanding of the reactions at hand, and to prepare the 2D simulations. Then, the 2D model simulated a horizontal stretch of aquifer, of 50 km length, and 30 km width, over a period of 10 000 a.

A massive, instantaneous, injection of CO_2 in the Dogger has been simulated with the reactive transport code Hytec. The amount of injected CO_2 has been chosen to represent the total amount of CO_2 produced by a powerplant over its entire life-time: a total 3×10^{11} kg, for an average production of 3 Mt·a^{-1} CO_2 over 100 years. Considering the pressure-temperature conditions, the supercritical CO_2 density is around 600 kg·m^{-3} (Air Liquide, 1976), so that it would occupy a total volume of 6.5×10^8 m^3 (considering a 25% porosity around the injection well). With a 200 m-thick aquifer, this would represent a (flat) cylinder (rather a pancake) of radius 1.78 km (*Fig. 4*).

The initial mineralogy has been prepared according to the data in Table 1. The pore water composition has been simulated by a 35 g/L NaCl solution, at pH 6.3, in equilibrium with the rock minerals. Hytec cannot account for two-phase flow. In a first approximation, the CO_2 injection has been represented by a fixed circular zone, of radius 1.78 km, with constant, high, dissolved-CO_2 content (see the discretization Figure 5). The concentration of the species CO_2(aq) has been fixed at 1.05 molal, corresponding to the solubility of the supercritical CO_2 under the conditions of the aquifer (pressure, temperature, salinity, data interpolated from Duan and Sun, 2002). The salinity in the bubble is the same as in the aquifer, and the pH has been fixed to 3 to take into account the acidification due to the acid gas injection. The pH is thus lower in the bubble than in the bulk of the aquifer. No mineral has been defined inside the bubble.

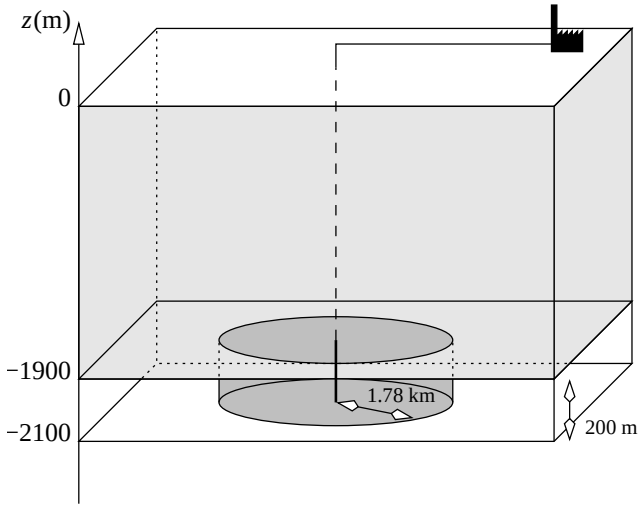

Figure 4

Schematic view of the instantaneous injection in the Dogger aquifer of the lifetime CO_2 production by a powerplant.

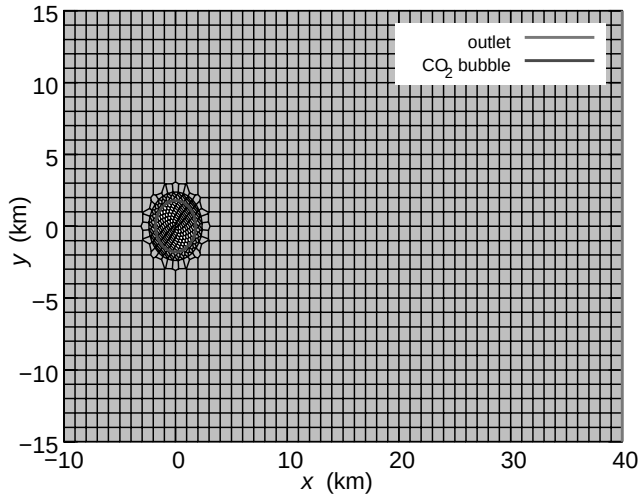

Figure 5

Discretization of the domain for the Dogger simulation; the central supercritical CO_2 bubble has been overgridded to enable a correct representation of the out-going CO_2 fluxes.

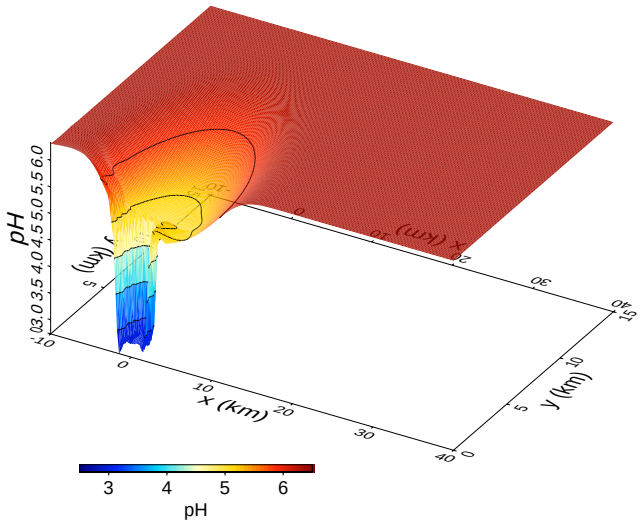

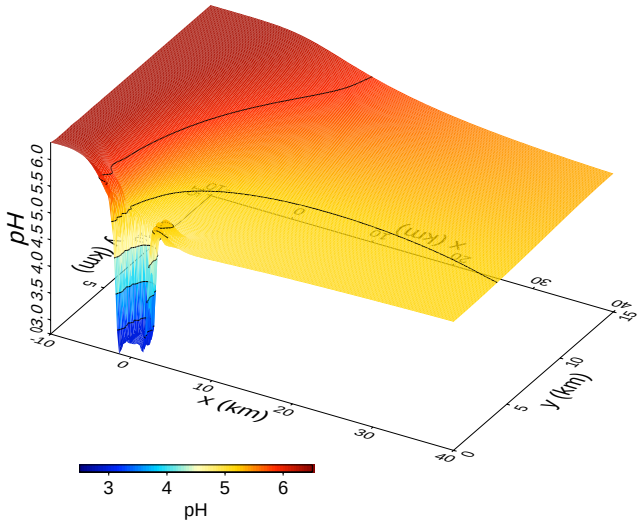

Figure 6

pH distribution for the first scenario of injection of supercritical CO_2 in the Dogger aquifer, at time 100 and 10 000 a. Small undershoots (lower than pH 3.0) can be seen around the bubble: these are due to incorrect interpollation by the post-processor, and do not appear on the profile Figure 7.

Several key points can be concluded from the simulation results.

– The pH evolves over large distances as the low pH in the CO_2 bubble enters the aquifer: see Figure 6 for the pH distribution (only $y > 0$), at time 100 and 10 000 a, or Figure 7 for a profile along the $y = 0$ axis. The diffusion/dispersion accounts for the spreading along the y-axis of the low pH zone.
– The CO_2 injected in the bubble flows through the aquifer: Figure 8 shows the profiles of the species CO_2(aq) and HCO_3^- and of the total dissoved CO_2 along a $y = 0$ axis at time 0, 500 and 10 000 a. The CO_2 distribution is also displayed in Figure 9, at time 200, 500, and 1 200 a.
– Calcite is very slowly dissolved during the evolution, starting at the edge of the bubble, downstream the aquifer, and, to a smaller extent, upwards (calcite concentration profiles on Figure 10). At time 10 000 a, the calcite is totally dissoved over a distance lower than 1 km.

To be more precise, the pH drops from an initial value of 6.3 to 4.8. The difference between the low pH in the bubble and the new pH in the aquifer is due to the calcite pH buffering. When the calcite is locally completely dissolved, the pH drops a second time, down to 3.

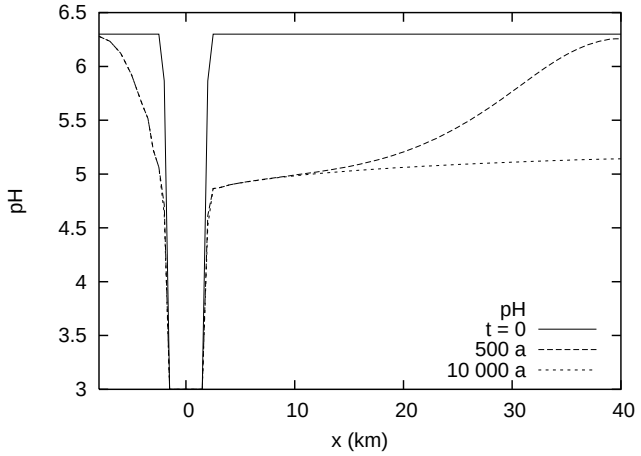

Figure 7

pH profiles ($y = 0$), for the first scenario of injection of supercritical CO_2 in the Dogger aquifer, at time 0, 500 and 10 000 a.

The concentration of the species CO_2(aq) has been fixed in the bubble zone. Due to the low pH, the carbonate system is dominated by the species CO_2(aq); HCO_3^- is 10^3 less concentrated than CO_2(aq). However, the pH buffering in the aquifer raises the pH so that the carbonate system moves towards more HCO_3^- favourable conditions: HCO_3^- is here around 0.05 mol/L. As a result, the total dissolved CO_2 is greater in the aquifer than in the bubble itself. Another phenomenon further increases the total dissolved CO_2: the pH buffering occurs at the expense of some calcite dissolution which feeds the medium with carbonates.

A dissolution front of dolomite can also be observed, moving at a similar velocity as the calcite dissolution front. On the contrary, pyrite does not seem to react over the time of the simulation.

3.2.2 Mass Balance

In order to evaluate the transport of dissolved CO_2 in the aquifer, a Hytec computation of the total dissolved CO_2 fluxes has been made through several control surfaces: at the input ($x = -10$ km) and exit ($x = 40$ km) boundaries and around the CO_2 bubble (*Fig. 11*). When a quasi stationary state is reached, the total dissolved CO_2 released from the bubble (on the whole 200 m layer) during the simulation has been estimated to 7×10^9 mol/a (therefore, the bubble would be completely depleted in about 975 a); taking the transient phase into account leads to a greater depletion time of 1 125 a.

The assumption of a constant bubble of supercritical CO_2 is therefore erroneous, and a more detailed simulation has to be devised.

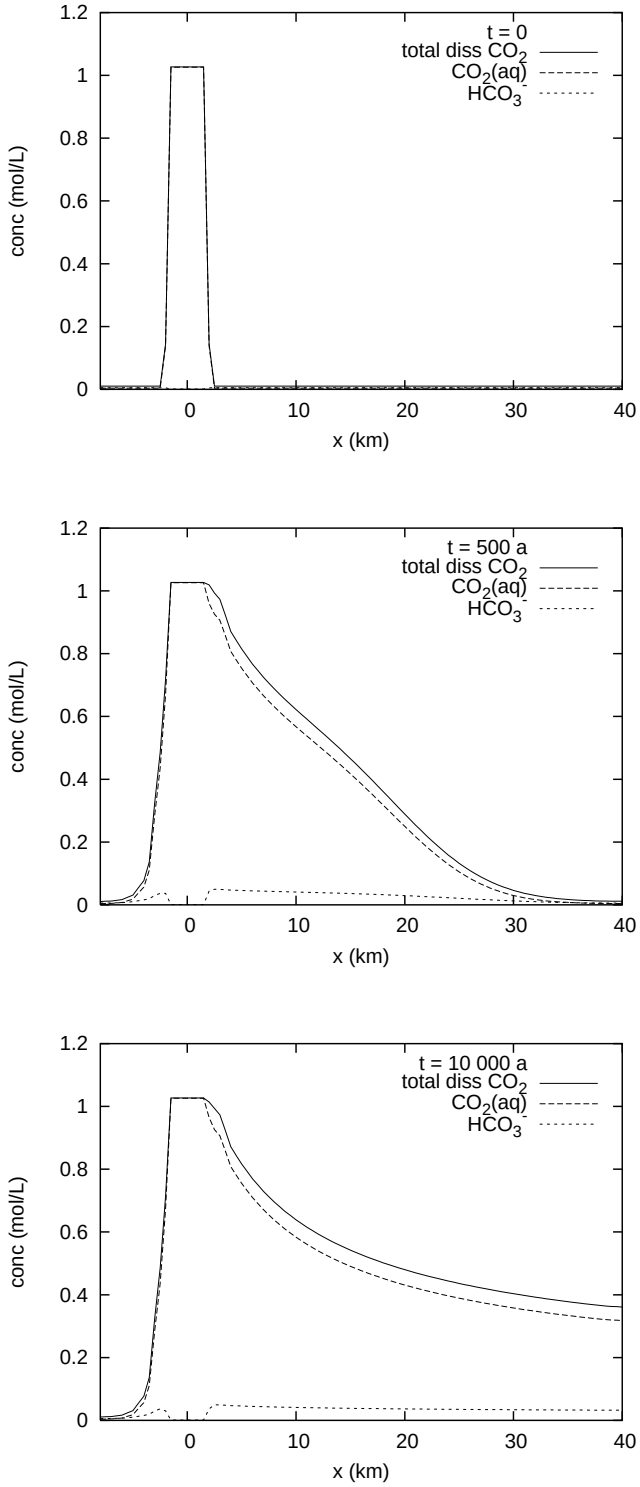

Figure 8

CO_2 concentration profiles ($y = 0$), for the first scenario of injection of supercritical CO_2 in the Dogger aquifer, at time 0, 500 and 10 000 a (the oscillations are due to the interpolation by the post-processor). The concentrations have been plotted for the species CO_2(aq) and HCO_3^- along with the total dissolved CO_2.

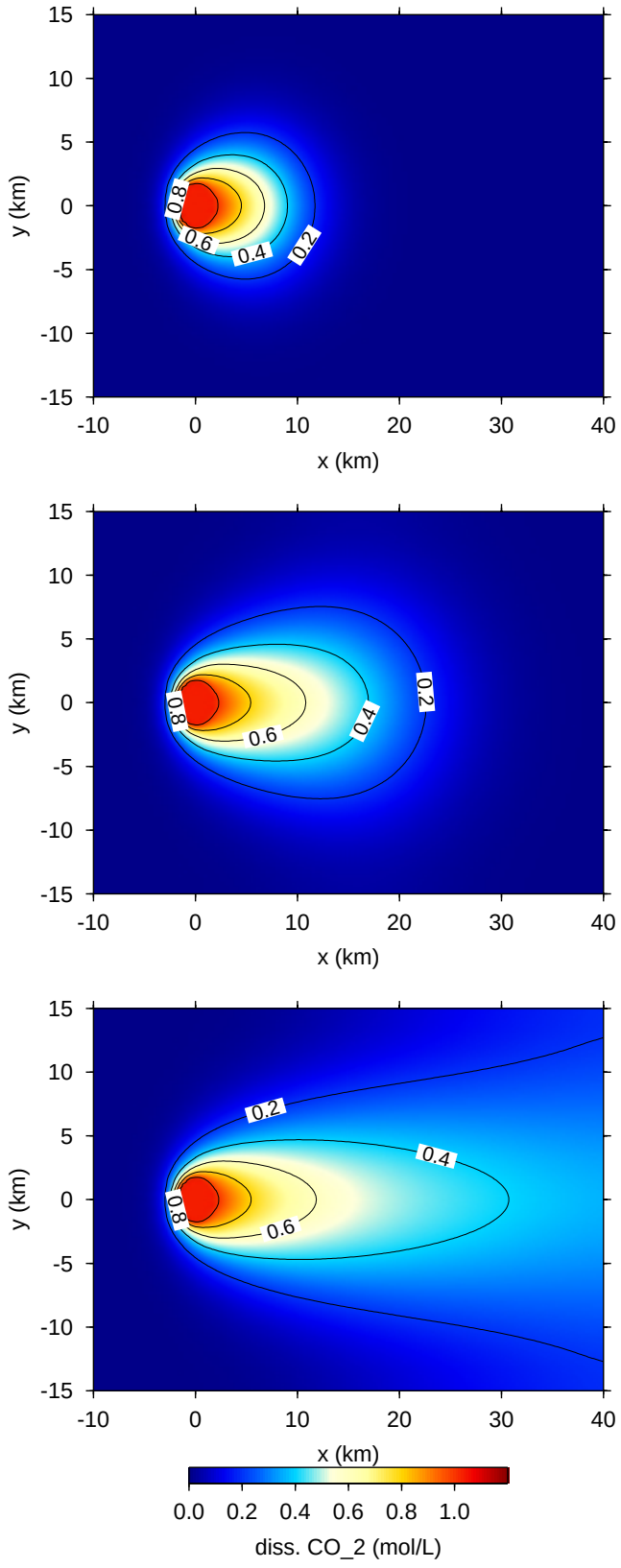

Figure 9

CO_2 distribution , for the first scenario of injection of supercritical CO_2 in the Dogger aquifer, at time 200, 500, and 1 200 a.

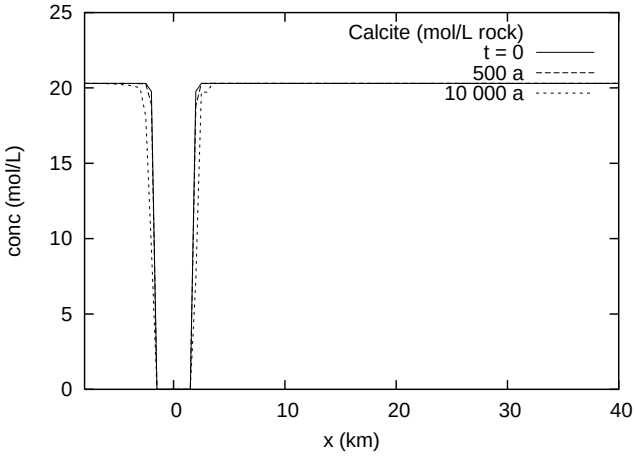

Figure 10

Calcite concentration profiles (in moles per unit volume of rock), for the first scenario of injection of supercritical CO_2 in the Dogger aquifer, at time 0, 500 and 10 000 a.

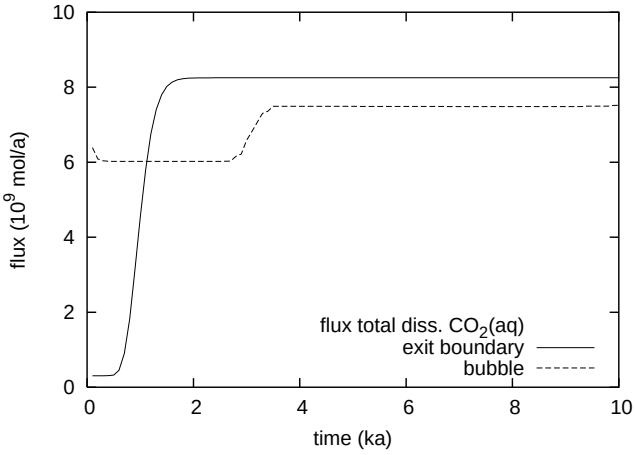

Figure 11

Total dissolved CO_2 fluxes through the exit boundary of the simulated aquifer, for the first scenario of injection of supercritical CO_2 in the Dogger aquifer.

3.2.3 Improved Model

The second model is based on the first simulation. However, two new phenomena are now taken into account:

- the CO_2 bubble is allowed to be depleted throughout the simulation, as the CO_2 is transported downstream the aquifer;
- the CO_2 bubble can also move downstream through the aquifer, due to the overall flow.

The initial system is identical to the previous one. The simulation is allowed to run for 200 a, then a mass balance on the released CO_2 is performed (cumulative flux of aqueous HCO_3^-); the new volume of the CO_2 bubble can

then be recalculated. Also, the center of the bubble is moved downstream in the aquifer, at a velocity 25 m/a, *i.e.* similar to the water pore flow velocity (38 m/a). The simulation is then resumed for a new period of 200 a until the bubble is completely depleted. In this way, the evolution of the CO_2 bubble is described by several successive CO_2 zones, which can be observed on the simulation grid (*Fig. 12*).

The improved simulation results are quite different from the first run. As the CO_2 bubble progresses through the aquifer, the source term of CO_2 and low pH also moves downstream through the aquifer (*e.g. Fig. 13* for pH).

Eventually, when the bubble is completely exhausted (at time $t = 1\,925$ a), no high CO_2/low pH constraint remains; the low pH water is flushed out of the simulated system, at the general flow velocity (*Fig. 13*, 2 000 a).

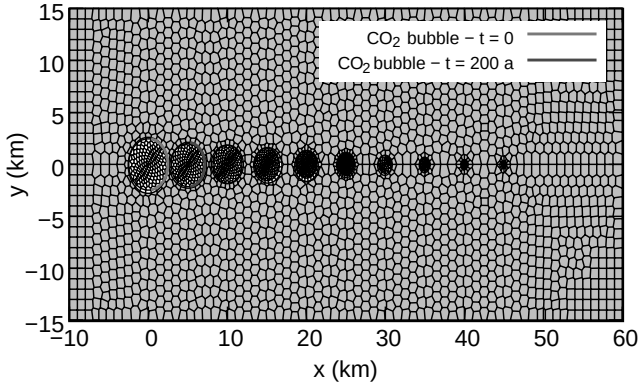

Figure 12

Discretization of the domain for the Dogger simulation, including the simulated progress (and depletion) of the supercritical CO_2 bubble.

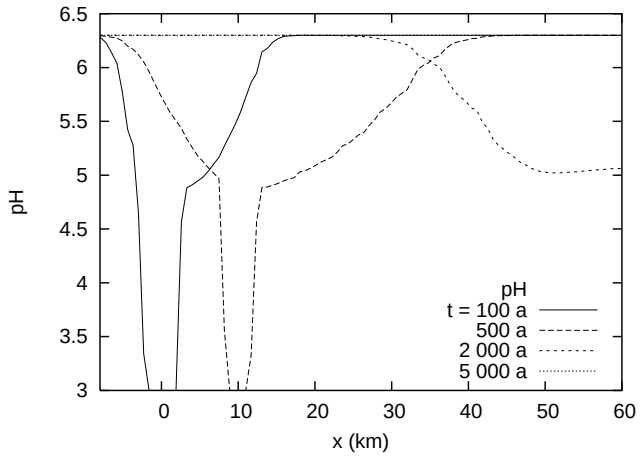

Figure 13

pH profiles ($y = 0$), for the improved scenario of injection of supercritical CO_2 in the Dogger aquifer, at time 100, 500, 2 000, and 5 000 a.

The behaviour of the carbonate system is very interesting, as shown in Figure 14 for various carbonate species profiles

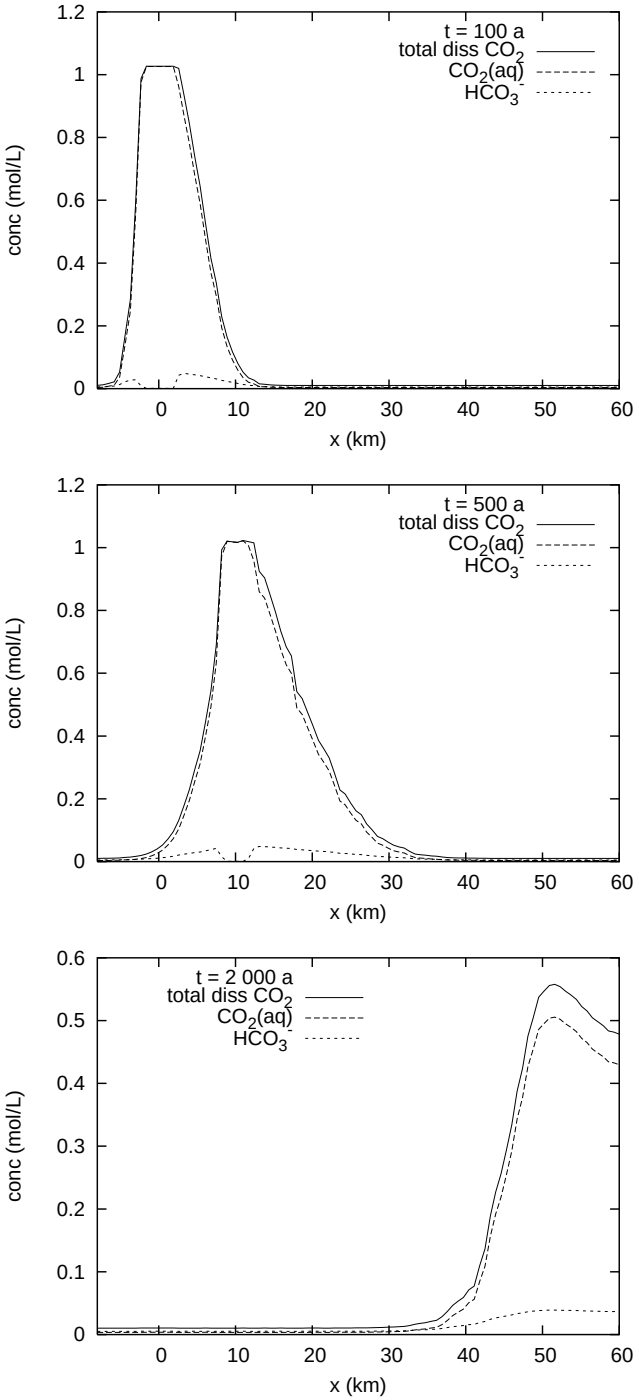

Figure 14

CO_2 concentration profiles ($y = 0$), for the improved scenario of injection of supercritical CO_2 in the Dogger aquifer, at time 100, 500 and 2 000 a. The concentrations have been plotted for the species CO_2(aq) and HCO_3^- along with the total dissolved CO_2.

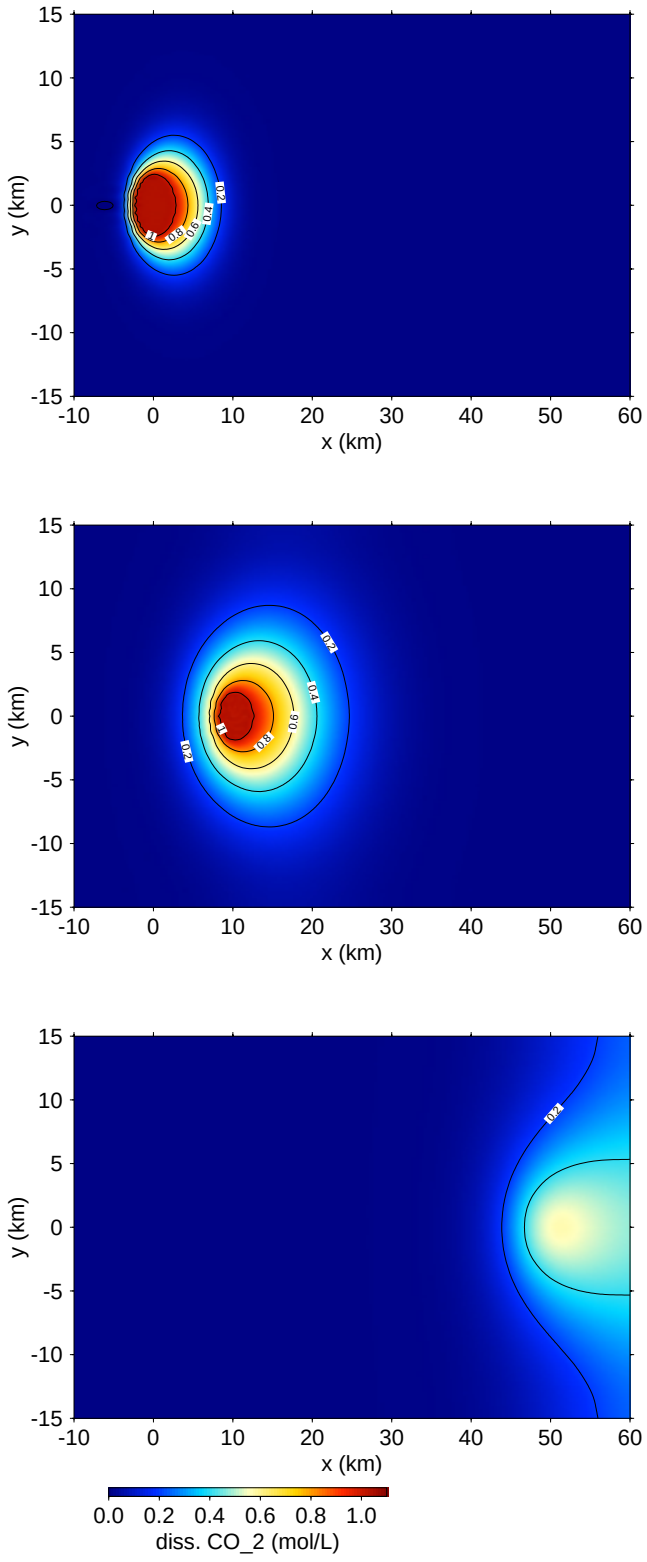

Figure 15

CO_2 distribution in the improved model for the Dogger 3.2.3, at time 200, 500, and 2 000 a, the last being 75 a after the exhaustion of the CO_2 bubble.

at different times, and in Figure 15 for the total dissolved CO_2 distribution at time 200, 500 and 2 000 a.

A slightly enhanced concentration in the total dissolved CO_2 can be observed, compared to the first simulation. The progress of the bubble is clearly visible from time 0 to time 500 a. In addition to the progress of the bubble through the aquifer, dissolved CO_2 is dispersed downstream the bubble: indeed, our assumption was that the bubble should flow less quickly than the water. A rather large CO_2 dispersion can be observed upstream the bubble at time 500 a: this is due to the flushing of the remnant of the first CO_2 bubbles, and is mainly due to our discrete approximated two-phase flow. Eventually, similar to the pH evolution, after the exhaustion of the bubble (around 2 000 a), the remaining CO_2 is flushed out of the system.

As in the first model, the calcite buffers the pH outside the bubble: the pH rises from 3 inside the bubble, to 4.8 just outside the bubble. This is achieved through the dissolution of part of the calcite: Figure 16 shows the distribution of the amount of calcite dissolved at time 5 000 a, *i.e.* after all the CO_2 injected in the bubble has been flushed out of the system. The dissolution occurs close to the limit of each discrete bubble; however, the dissolution is rather limited, as a maximum of 1.04 mol/L of calcite is dissolved out of an initial 20.3 mol/L (concentrations in mol/L of rock). The dissolution is thus much reduced compared to the first simulation; a complete two-phase flow simulation would certainly further reduce the maximum dissolved calcite, with a more homogeneous flow of the bubble.

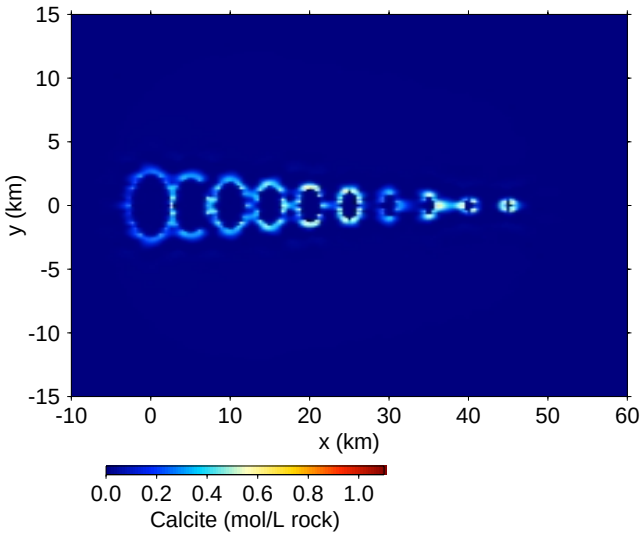

Figure 16

Calcite dissolution due to the CO_2 injection (in moles per unit volume of rock) at time 5 000 a, for the improved scenario of injection of supercritical CO_2 in the Dogger aquifer.

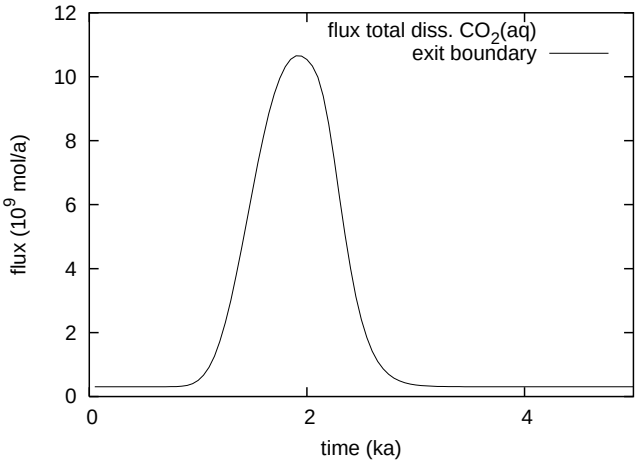

Figure 17

Total dissolved CO_2 fluxes through the exit boundary of the simulated aquifer, improved Dogger simulation.

The flux of total dissolved CO_2 out of the simulated system is represented in Figure 17. The flux has been calculated at a distance 60 km from the CO_2 injection point. It appears that the great majority of the CO_2 is flushed out of the simulated part of the aquifer in less than 2 500 a, with a peak around 2 000 a. The main sequestering effect is thus a 1 000 a delay at a distance 60 km from the injection point, but in the end, the whole CO_2 is flushed out of the simulated part of the aquifer.

3.3 Discussion

Two models of the massive injection of CO_2 into the Dogger aquifer have been performed. The simulation results show that a small increase in the solubility of CO_2 can be expected in carbonated aquifers, due to the relatively high pH buffering of the carbonated minerals. The increase is of the order of 10% in the present simulation but is strongly dependent on the local pH. The pH buffering occurs at the expense of some carbonated mineral dissolution; this effect further increases the amount of dissolved CO_2 in the pore water, which is not what is demanded of the sequestration. However, the amount of carbonates dissolved remains rather low (around 5% of the initial calcite), which should prevent major modifications of the aquifer properties (mechanical, *etc.*).

The description of the supercritical CO_2 bubble was the main concern in the simulations. The bubble has been approximated using a constant (dissolved) CO_2(aq) concentration area. The first 10 000 a simulation revealed that the CO_2 bubble would evolve due to the leakage of CO_2 in the aquifer: indeed, a simple mass balance indicates that the bubble would be completely depleted (*i.e.* completely dissolved) in less than 1 200 a. The second model attempted to assess the problem in a more detailed way: the CO_2 bubble was allowed to be progressively depleted (following the transport of CO_2 throughout the aquifer) and to move through the aquifer, due to the general flow.

These attempts to simulate the CO_2 bubble highlight the limitations of the reactive transport code. The problem would be accurately addressed by a fully coupled two-phase flow reactive transport model. Besides, a coupling between the composition of each phase, including the possibility to dissolve CO_2 into the water phase (or water into the supercritical CO_2 phase), would be required.

From the point of view of CO_2 sequestration efficiency, it appears that the CO_2 is completely flushed out of the system, with a delay and a dispersion depending on the distance from the injection point and the properties of the aquifer. Thus, the sequestration efficiency resides mainly in the long residence time of the aquifer (slow velocity and/or a distant outcrop). Nevertheless, the high dissolution capacity of the aquifer is a positive point, since the behaviour of the supercritical CO_2 phase is still largely unknown.

4 SANDSTONE AQUIFER MODEL

4.1 Description of the Aquifer

The Bunter sandstone aquifer (North Sea) has been selected on similar criteria to the carbonated aquifer. It is located in the North Sea, 300 km north of the French coastline (Dunkerque). The aquifer is composed of Buntsandstein sandstone, that settled in the lower Trias from 325 to 230 Ma BP, in a continental environment on the West border of the large Triasic German Basin. It has been covered by 1 000 m of calcareous and marly sediments of medium Trias to upper Jurassic, that constitute a 300 m-thick impermeable caprock. The impermeable bedrock is composed of Permian marls, salts and anhydrite. The aquifer is mainly composed of silicates (quartz, annite) and feldspar. Its pore water is very saline, around 300 g/L NaCl.

Its properties and mineral composition are summarized in Table 2. The Bunter aquifer is less well characterized than the Dogger; in particular, its mineral composition has been infered from outcrops in eastern England and the Black Forest (Germany). An arbitrary Darcy flow velocity of 0.1 m/a as been chosen; in these conditions, the dominant transport process is diffusion.

4.2 Model for the Bunter

An instantaneous injection of 3×10^{11} kg of CO_2 in the Bunter aquifer has been simulated. Like in the Dogger simulation, the CO_2 is represented as a bubble of constrained CO_2(aq) concentration: $[CO_2(aq)] = 0.46$ molal (data extrapolated from Duan and Sun, 2002); with a thickness of 100 m and a local enhanced porosity of 25% in the injection zone, the radius of the CO_2 cylindrical bubble is thus 2.52 km (discretization grid Figure 18). The problem of the description of the

TABLE 2

Physical, hydrological and chemical properties of Bunter aquifer. The mineral composition is given in weight percent.

Physical properties	
Average depth	1 800 m
Average thickness	100 m
Surface area	700 km^2
Density	2.21 kg/m^3
Temperature	66 °C
Pressure	157 bar
Hydrological properties	
Porosity	$\sim$ 20%
Permeability	5×10^{-6} m/s
Mean Darcy flow velocity	< 0.1 m/a
Chemistry	
Salinity	303 g/L NaCl
Mineral composition	
Quartz	49.5%
Annite	24%
Feldspar	12.5%
Nontronite	4%
Calcite	3%
Hematite	3%
Dolomite	3%
Pyrite	1%

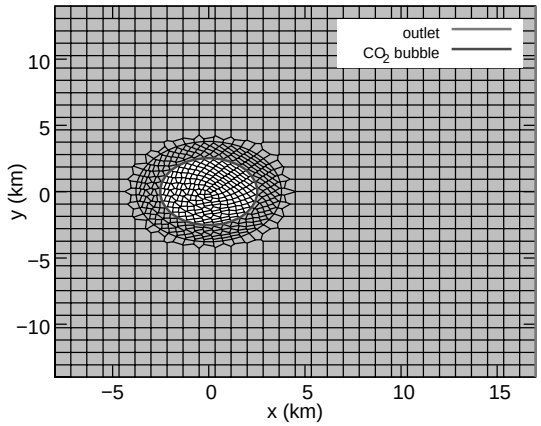

Figure 18

Discretization grid for the Bunter simulation. The CO_2 injection zone has been overgrided to ensure a more accurate computation of the outgoing dissolved CO_2 fluxes.

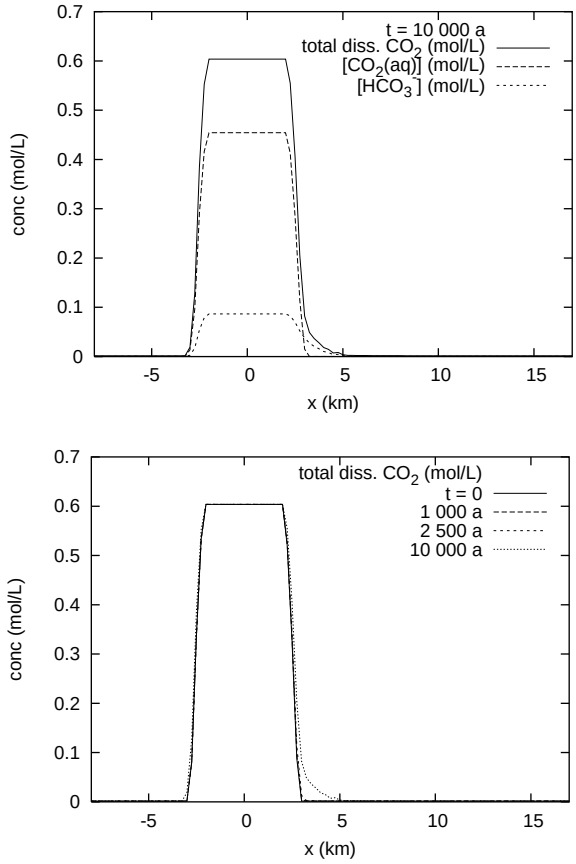

Figure 19

Carbonate species profiles ($y = 0$), for the scenario of injection of supercritical CO_2 in the Bunter aquifer, at time 10 000 a (top), and total dissolved CO_2 at time 0, 1 000, 2 500, and 10 000 a (bottom). The dissolved CO_2 is in great part sequestred within a very close range around the supercritical CO_2 bubble.

CO_2 bubble arises as in the Dogger simulation. However, the very slow general flow limits the depletion and the movement of the bubble, so that the constrained CO_2(aq) approximation is better in this case.

The simulation results are more abundant in this case than in the Dogger simulations. Indeed, the geochemistry is more complex and leads to an effective mineral sequestration of the CO_2 (*Fig. 19*): the high total dissolved CO_2 concentration is confined within a close range around the supercritical bubble, even after a long evolution (10 000 a).

Indeed, immediately downstream the supercritical CO_2 bubble, the total CO_2 concentration is cut by a factor 8, and drops even lower further on in the aquifer.

As the CO_2 is released by dissolution of the supercritical CO_2 bubble, it is transported within the aquifer, where it can react with the various primary minerals. The main reaction is thus

$$\text{annite} + 3\,CO_2(\text{aq}) \rightleftharpoons 3\,\text{siderite} + \text{K-feldspar}, \qquad (9)$$

with a reaction constant $\log K(60\,^\circ\text{C}) = 9.09$. The reaction can be followed on the mineral profiles (*Fig. 20*, *21*).

The reaction between annite and CO_2 is responsible for the drop in CO_2 concentration down to 0.08 mol/L. When the annite is exhausted in a discretization cell, the secondary

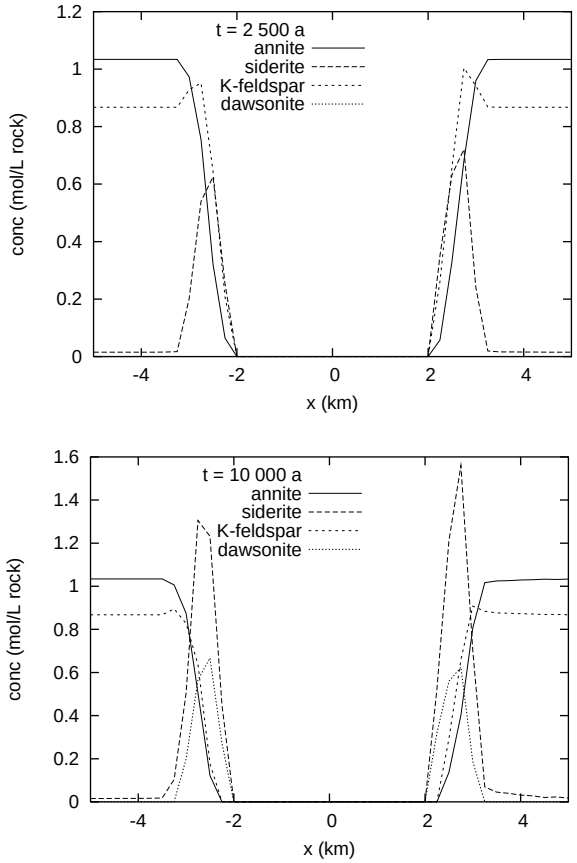

Figure 20

Mineral concentrations profile at time 2 500 and 10 000 a. Annite is dissolved by the CO_2 front and allows for the formation of secondary siderite and K-feldspar. When the annite is exhausted, the K-feldspar starts dissolving and form dawsonite (and quartz).

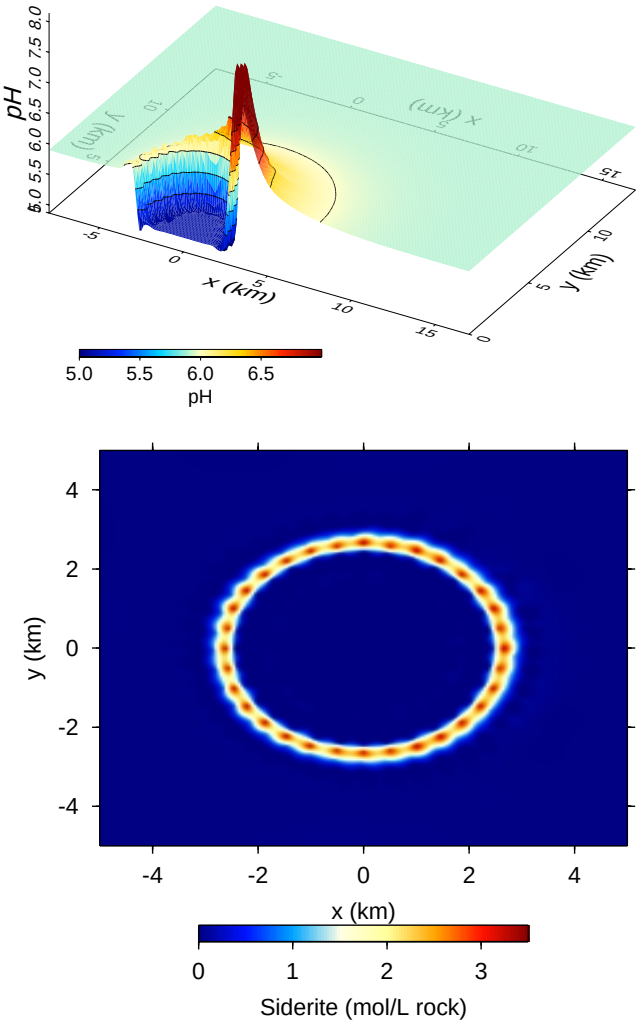

Figure 21

pH and Annite (in moles per unit volume of rock) at time 10 000 a, for the scenario of injection of supercritical CO_2 in the Bunter aquifer.

minerals start reacting:

$$\text{K-feldspar} + CO_2(\text{aq}) + Na^+ \leftrightharpoons \text{dawsonite} + 3\,\text{Quartz} + K^+ \quad (10)$$

although siderite remains stable. In this region, the dissolved CO_2 is around 0.2 molal. The overall result is a dissolution of the primary annite and a mineral sequestration of CO_2 as siderite and dawsonite, with precipitation of quartz and transient K-feldspar.

The mineralogical evolution is correlated with a modification of the pH (*Fig. 22*). A rise in the pH downstream the bubble can be observed. Surprisingly, the pH is higher in the reacting zone than in both undisturbed areas: pH is 5.1 in the CO_2 bubble, 5.9 in the undisturbed aquifer, but rises to 7.7 in the reaction zone. This effect is due to the modification of the concentration in Fe^{2+}, which is lowered at the reaction front by the precipitation of siderite. But iron is a constituant

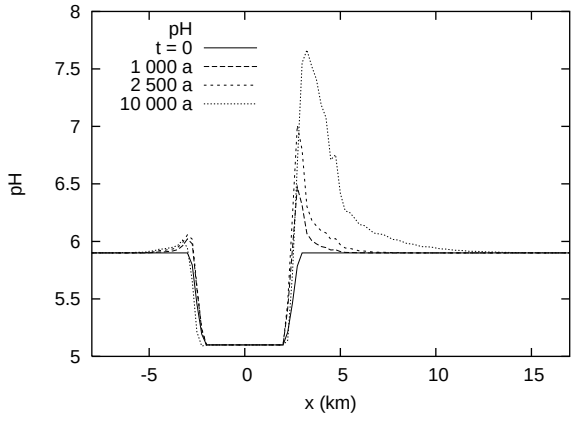

Figure 22

pH profiles ($y = 0$) at time 0, 1 000, 2 500, and 10 000 a for the Bunter simulation.

of annite:

$$\text{annite} + 10H^+ \rightleftharpoons Al^{3+} + K^+ + 3\,SiO_2(aq) + 3\,Fe^{2+} + 6H_2O. \quad (11)$$

Since Al, Si, and K do not change dramatically at the reacting front, and in presence of annite, a drop in the Fe^{2+} concentration leads to a drop in the H^+: the drop in Fe^{2+} concentration in the solution increases the equilibrium pH of annite in the system.

The other minerals in the system display less interesting features. A slow dissolution front of Calcite can be observed around the border of the bubble, followed by a reprecipitation front inside the aquifer, due to the higher local pH. Pyrite and the other minerals do not seem to react in the first 10 000 years of simulation.

Finally, the porosity does not evolve significantly, with a drop from 20% inside the aquifer to 18.5% around the bubble. However, a local modification of the flow and transport parameters might occur, depending on the precise location of the precipitates inside the pore structure.

4.3 Discussion

The simulation shows a greater impact of the geochemistry in this case than in the Dogger simulation. The evolution of the concentration in dissolved CO_2 is dominated by the effect of several mineralogical reactions, mainly the mineral trapping of CO_2 which forms siderite and dawsonite when reacting with annite. As a result, the dissolved CO_2 is very efficiently confined within a short range around the supercritical CO_2 bubble. Indeed, the aquifer remains almost undisturbed at a distance over 10 km from the CO_2 injection point even after 10 000 a of simulation. The result is a very efficient mineralization of the CO_2, which ensures a good sequestration even over geological time scales.

The problem of the description of the supercritical CO_2 bubble is not as critical here as in the Dogger simulation, for two main reasons:

– the general flow is much slower;
– the main controlling process here is the reaction of the dissolved CO_2 with the rock minerals.

However, the reactivity of the supercritical CO_2 in contact with the host rock should be assessed, to check if any major reaction can occur within the bubble. These reactions may potentially consume a part of the CO_2 (which is rather positive from a sequestration point of view) but it could also lead to an alteration of the rock and of its confining properties.

The major problem in this simulation was the lack of data, both on the aquifer itself and the reaction constants under sequestration conditions (temperature, pressure). Finally, a kinetic control is likely to occur, especially for the reputedly slow silicates, which will be addressed in future simulations.

CONCLUSION

This paper aimed at assessing the advantages and limitations of reactive transport codes in the field of CO_2 sequestration studies. Several simulations were conducted to illustrate the possibilities and the difficulties in modelling the massive injection of CO_2 in deep saline aquifers.

Injections in a carbonated aquifer and a sandstone aquifer have thus been simulated. The results are encouraging. The evolution of the dissolved CO_2 has been successfully described, with a coupling between transport and chemical reactions. It has been shown that transport controlled the dispersion of the dissolved CO_2 in the carbonated aquifer, with a quick dissolution of the whole supercritical CO_2 bubble (enhanced by the pH buffer capacity of the host rock carbonated minerals), and a transport of all the injected CO_2 bubble in the flow direction.

In the case of the sandstone aquifer, the evolution is controlled by the reactivity of the dissolved CO_2 with the host rock minerals. The dissolution of silicates enables the precipitation of new carbonated minerals, so that very efficient mineral trapping (on geological time scales) is ensured. In addition, the dissolution of the CO_2 bubble is much slower, partly due to the lower general flow rate of the aquifer.

Thus, reactive transport codes can effectively simulate CO_2 sequestration scenarios. They actively couple transport and geochemical processes, which enables a better understanding of the system (compared to separated transport modelling and geochemical modelling). They also allow for a correct assessment of the flux of dissolved CO_2 throught predefined boundaries (*e.g.* the limit of the CO_2 bubble or the end of the aquifer), which is a good, readily understandable, estimator of the trapping capacity of the system.

However, several key points need further investigation. Some of them can be quite easily addressed, as they involve common investigation techniques. This includes a better description of the aquifers (the aquifers are chosen for their poor economic value, which explain why few investigations have been carried out on them so far), a refining of the thermodynamic data under the appropriate P-T conditions, and in some cases of the associated kinetic data (especially for silicates).

Some points need more careful attention though. The approximate description of the supercritical CO_2 bubble reached its limits in the carbonated aquifer model. A correct description of the evolution of the bubble is thus desirable in terms of transport and depletion of the bubble. This involves a fully coupled two-phase flow reactive transport, with a correct assessment of the crossed dissolution between phases.

Finally, the reactivity of the supercritical CO_2 with the host rock minerals should also be (at least) assessed. Despite the poor ionic solvant capacity of supercritical CO_2, its activity may not be negligible. In this case, the reactions ought to be expressed mathematically and implemented in

the simulation codes. However, to our knowledge, no data are available yet.

In view of the problems raised by these preliminary simulations, it has been decided to launch some developments in the Hytec code. A two-phase flow module is being developed within R2D2 to better describe the hydrodynamics of the sequestration systems and particular attention will be given to the coupling with the chemistry.

ACKNOWLEDGEMENTS

This study was realized by Aurélie Pipart as a part of her post-graduate work, at the *École des mines de Paris*, with financial support of *Électricité de France*.

REFERENCES

1 Air Liquide (1976) *Encyclopédie des gaz, gas encyclopaedia*, Elsevier, Amsterdam.

2 Bachu, S. (2002) Sequestration of CO_2 in geological media in response to climatic change: road map for site selection using the transform of the geological space into CO_2 phase space. *Energy Conversion and Management*, **43**, 87-102.

3 Bachu, S., Gunter, W., and Perkins, E. (1994) Aquifer disposal of CO_2: hydrodynamic and mineral trapping. *Energy Conversion and Management*, **35**, 269-279.

4 Brønsted, J. N. (1922) Studies on solubility. IV. The principle of the specific interaction of ions. *Journal of the American Chemical Society*, **44**, 877-898.

5 Carrayrou, J., Mosé, R., and Behra, P. (2002) Comparison of mass balance errors in operator-splitting procedures for reactive transport. *Journal of Contaminant Hydrology*, **68**, 239-268.

6 Duan, Z. and Sun, R. (2002) An improved model calculating CO_2 solubility in pure water and aqueous NaCl solutions from 273 to 533 K and from 0 to 2000 bar. *Chemical Geology*, **193**, 257-271.

7 Fein, J.B. and Walter, J.V. (1987) Calcite solubility in supercritical CO_2-H_2O fluids. *Geochimica et Cosmochimica Acta*, **51**, 1665-1673.

8 Gaus, I., Azaroual, M., and Czernichowski-Lauriol, I. (2003) Reactive transport modelling of dissolved CO_2 in the cap rock base during CO_2 sequestration (Sleipner site, North Sea). *Second Annual Conference on Carbon Sequestration*, may 5-8th, http://www.iku.sintef.no/projects/IK23430000/Publications/Gaus_etal_CarbonSeqIIConf.pdf.

9 Gunter, W., Perkins, E., and McCann, T. (1993) Aquifer disposal of CO_2-rich gases: reaction design for added capacity. *Energy Conversion and management*, **34**, 941-948.

10 Gunter, W., Wiwchar, B., and Perkins, E. (1997) Aquifer disposal of CO_2-rich greenhouse gases: extension of the time scale of experiment for CO_2-sequestering reactions by geochemical modelling. *Mineralogy and Petrology*, **59**, 121-140.

11 Helgeson, H. (1969) Thermodynamics of hydrothermal systems at elevated temperatures and pressures. *American journal of science*, **267**, 729-804.

12 Hundsdorfer, W. and Verwer, J.G. (1995) A note on splitting errors for advection–diffusion-reaction equation. *Applied Numerical Mathematics*, **18**, 191-199.

13 Johnson, J.W., Nitao, J.J., Steefel, C., and Knaus, K.G. (2001) Reactive Transport Modeling of Geologic CO_2 Sequestration in Saline Aquifers; The Influence of Intra-Aquifer Shales and the Relative Effectiveness of Structural, Solubility, and Mineral Trapping During Prograde and Retrograde Sequestration. *First Annual Conference on Carbon Sequestration*, may 14-17th, 2001, http://www.netl.doe.gov/publications/proceedings/01/carbon_seq/P28.pdf

14 Joyce, D.B. and Holloway, J.R. (1993) An experimental determination of the thermodynamic properties of H_2O-CO_2-NaCl fluids at high pressures and temperatures. *Geochimica et Cosmochimica Acta*, **57**, 733-746.

15 Kaszuba, J., Janecky, D., and Snow, M. (2003) Carbon dioxide reaction processes in a model brine aquifer at 200 °C and 200 bars: implications for geologic sequestration of carbon. *Applied Geochemistry*, **18**, 1065-1080.

16 Lagneau, V. (2003) R2d2 – Reactive Transport and Waterflow on an Odd Dimension 2 grid, Notice technique et vérification. *Technical Report No. LMH/RD/03/05*, École des mines de Paris, Paris, http://www.cig.ensmp.fr/~lagneau/docr2d2.pdf.

17 Leitner, W. (2000) Homogeneous catalysts for application in supercritical carbon dioxide as a 'green' solvent. *Compte-rendu de l'Académie des sciences*, **3** (special issue on "Green Chemistry"), 595-600, Paris.

18 Li, Q., Zhang, Z., Zhong, C., Liu, Y., and Zhou, Q. (2003) Solubility of solid solutes in supercritical carbon dioxide with and without cosolvents. *Fluid Phase Equilibria*, **207**, 183-192.

19 Lichtner, P.C. (1996) Continuum formulation of multicomponent-multiphase reactive transport, in *Reactive transport in porous media*, Lichtner, P.C., Steefel, C., and Oelkers, E.H. *editors*, Reviews in mineralogy, **34**, Mineralogical Society of America, 1-81.

20 Pruess, K., García, J., Kovscek, T., Oldenburg, C., Rutqvist, J., Steefel, C., and Xu, T. (2002) Intercomparison of numerical simulation codes for geologic disposal of CO_2 *Technical report* Lawrence Berkeley Laboratory report LBNL-51813, report available at http://www-esd.lbl.gov/GEOSEQ/code/pdfs/LBNL_51813.pdft.

21 Pruess, K., García, J., Kovscek, T., Oldenburg, C., Rutqvist, J., Steefel, C., and Xu, T. (2004) Code intercomparison builds confidence in numerical simulation models for géologic disposal of CO_2. *Energy*, **29**, 1431-1444.

22 Reichle, D., Houghton, J., Kane, B., and Ekmann, J. (1999) Carbon sequestration research and development. *Technical Report*, Office of Science, Office of Fossil Energy, U.S. Department of Energy, report available at http://www.ornl.gov/carbon_sequestration/.

23 Rochelle, C., Pearce, J., and Holloway, S. (1999) The underground sequestration of carbon dioxide: containment by chemical reactions in the deep geosphere. In: Metcalfe, R., Rochelle, C. (Eds.), *Chemical Containment of Waste in the Geosphere*, special publication, The Geological Society of London, **157**, 117-129.

24 Steefel, C. and Lasaga, A. (1994) A coupled model for transport of multiple chemical species and kinetic precipitation/dissolution reactions with application to reactive flow in single phase hydrothermal systems. *American Journal of Science*, **294**, 529-592.

25 Steefel, C. and MacQuarrie, K. (1996) Approaches to modeling of reactive transport in porous media, in *Reactive transport in porous media*, Lichtner, P., Steefel, C.., and Oelkers, E. *editors*, Reviews in mineralogy, **34**, Mineralogical Society of America, 83-129.

26 van Cappellen, P. and Wang, Y. (1996) Cycling of iron and manganese in surface sediments: a general theory for the coupled transport and reaction of carbon, oxygen, nitrogen, sulfur, iron and manganese. *American Journal of Science*, **296**, 197-243.

27 van der Lee, J. (1997) Modélisation du comportement géochimique et du transport des radionucléides. *Ph.D. thesis*, École nationale supérieure des mines de Paris.

28 van der Lee, J. (1998) Thermodynamic and mathematical concepts of Chess. *Technical Report No. LHM/RD/98/39*, École des mines de Paris, Paris, http://chess.ensmp.fr/download/concepts.pdf.

29 van der Lee, J. and De Windt, L. (2001) Present state and future directions of modeling of geochemistry in hydrogeological systems. *Journal of Contaminant Hydrology*, **47**, 265-282.

30 van der Lee, J., De Windt, L., Lagneau, V. and Goblet, P. (2002) Presentation and application of the reactive transport code Hytec. *Computational Methods in Water Resources*, **1**, 599-606.

31 van der Lee, J., De Windt, L., Lagneau, V. and Goblet, P. (2003) Module-oriented modeling of reactive transport with hytec. *Computers & Geosciences*, **29**, 265-275.

Final manuscript received in March 2004